



Material-structure-process-performance integrated optimization method of steel/aluminum self-piercing riveted joint

Chong Xie^{1,2} · Dengfeng Wang³ · Dewen Kong³ · Shuang Wang⁴ · Changqing Du^{1,2}

Received: 8 June 2023 / Accepted: 19 March 2024 / Published online: 26 March 2024
© The Author(s), under exclusive licence to Springer-Verlag London Ltd., part of Springer Nature 2024

Abstract

To improve the reliability of the connection of various steel/aluminum dissimilar materials, an integrated optimization method of material-structure-process-performance is proposed to realize the optimal design of process parameters. First, the Johnson–Cook material model and failure fracture model are established to ensure the accuracy of the simulation model. Then, an integrated simulation analysis for self-piercing riveted joint forming and tensile mechanical performance is established considering the residual information of the joint forming process. Compared with the experimental results, the accuracy of the established model is higher than the model without considering the residual information. Finally, a hybrid sequence approximate optimization that comprehensively considers the forming quality and tensile mechanical performance is constructed to determine the optimal riveting parameters. Compared with the initial design, the maximum pull-out force, maximum shear force, and maximum peeling force of the optimized design for DC01 and 5754 rivets are increased by 35.66%, 8.6%, and 22.43%, respectively, and the maximum pullout force, maximum shear force and maximum peeling force of the optimized design for HC280 and 5754 rivets are increased by 1.490%, 1.292%, and 6.867%, respectively. Moreover, the accuracy and efficiency of self-piercing riveting process design are improved.

Keywords Self-piercing riveting · Failure model · Residual information · Sequence approximate optimization

1 Introduction

With the development of automotive lightweight technology, steel and aluminum alloy materials are widely used in mixed material body. But the traditional fusion welding process tends to form hard and brittle intermetallic compounds when joining materials of steel and aluminum alloy, which leads to poor joint reliability [1]. To solve this problem, a

variety of reliable joining processes for dissimilar materials have been proposed, such as self-piercing riveted technology (SPR) [2], flow drill screwing technology [3], and clinch riveting [4]. Among them, SPR can not only realize the riveting between sheets with the same material properties, but realize the connection between sheets of different materials and different thicknesses. Moreover, the riveting quality and reliability are high, so it is often used for the connection of steel and aluminum materials in the car body [5, 6].

Research on SPR often uses experimental methods to evaluate the quality of riveted joints [7, 8]. Compared with experimental methods, SPR's finite element simulation provides a more direct way to discover the joint deformation and damage mechanism [9, 10]. But a high-precision SPR joint simulation is crucial to obtain the mechanical performance of the joint. Common mechanical performance evaluations of SPR joints include three working conditions: shearing, cross-drawing, and peeling. Porcaro and Hansen et al. [11, 12] studied the SPR of 6060-T6 and 6060-T4 aluminum sheets with different thicknesses via the finite element method. A solid finite element model (FEM) was established to simulate the drawing condition. A comparison

✉ Chong Xie
chongxie@whut.edu.cn

¹ Hubei Key Laboratory of Advanced Technology for Automotive Components, Wuhan University of Technology, Wuhan 430070, People's Republic of China

² Hubei Collaborative Innovation Center for Automotive Components Technology, Wuhan University of Technology, Wuhan 430070, People's Republic of China

³ State Key Laboratory of Automotive Simulation and Control, College of Automotive Engineering, Jilin University, Changchun 130022, People's Republic of China

⁴ Huanghe Science and Technology University, Zhengzhou 450006, People's Republic of China

of simulation and test results shows that the riveted sheet undergoes large plastic deformation or even tearing, resulting in large load force and failure displacement. The main reason for this result is that the model ignores material failure modes. Xue et al. [13] prepared equivalent specimens of sheets with different pre-strain levels by flat rolling process. The effect of considering riveting forming strain on the prediction accuracy was discussed by studying the mechanical performance of SPR joints between DP590 high-strength steel and AC43500-T7 cast aluminum alloy sheets. The prediction accuracy of the pre-strained joint is improved. Therefore, it is very important to consider the material failure model of the riveted sheet and the residual information (stress and strain, etc.) during the rivet forming process [14].

Since the parameters of rivets and dies affect the forming quality and mechanical performance of SPR joints, some scholars have studied the effect of different parameters on different performances to obtain the best structural parameters [15]. Jin et al. [16] carried out SPR of DP590 high-strength steel and 6061T6 aluminum alloy sheets. The influence of process parameters on the riveting forming quality and shear strength were analyzed, such as the height of boss, diameter of die, and length of rivets. The process parameters were optimized by the orthogonal experiment method, and the best combination of rivet length and die parameters was determined. The experimental design optimization method can only find the best combination of set parameters, but it is difficult to find the optimal solution. The calculation efficiency is low.

To improve the optimization efficiency and find the optimal solution, the optimization method based on the static approximate model is applied to the analysis of the forming and tensile mechanical performance of SPR joints. Zhao et al. [17] developed two regression models to predict the joint forming quality and systematically analyzed the influence of rivet and die parameters on joint interlock and remaining thickness, indicating the accuracy of the prediction model. Zhang et al. [18] determined the range of rivet and die parameters through sensitivity analysis, and established the relationship between process parameters and joint forming indicators using the response surface model (RSM). The optimization is carried out by using the genetic algorithm, and the rivet and die parameters of the optimal joint forming parameters are determined. Zhao et al. [19] used an artificial neural network to predict the quality of SPR joints. Combined with a genetic algorithm, the parameters of rivet and die can be quickly determined. Fang et al. [20] proposed a framework integrating machine learning and global sensitivity analysis to optimize the parameters of SPR simulation analysis. Wang et al. [21] established a 3D FEM of SPR. Combined with the multi-criteria decision-making method, the process parameters of SPR joints are optimized, which improves the mechanical performance of the joints. The above research on SPR joints

shows that the approximate model is effective in predicting the forming quality of SPR and the mechanical performance of joints. However, as the number and range of joint parameters increase, the changing trend of the joint quality evaluation index will become highly nonlinear. The simulation analysis of the forming and tensile mechanical performance of SPR joints is time-consuming and computationally inefficient. There are many kinds of steel-aluminum dissimilar material connections in the mixed material body, so the optimization method based on the static approximate model will be difficult to efficiently obtain the joint process parameters of the optimal mechanical performance. The sequence approximate optimization method is iteratively calculated by coupling the approximate model and optimization algorithm and eliminates the step of accuracy testing [22]. The sequential approximate optimization method provides an efficient optimization method.

This paper proposes a structure-process-performance integrated optimization method for SPR connection joints of various dissimilar materials to quickly obtain the optimal process parameters of SPR connection. The main content of this paper is as follows: In Section 2, the constitutive relationship of the riveted sheet material and the mechanical performance test of the joint are carried out. In Section 3, the integrated simulation analysis of the forming-tensile mechanical performance of the SPR joint considering the post-forming information is carried out. The SPR joint material-structure-process-performance integrated sequential approximate optimization method is studied in Section 4. Finally, the conclusions are summarized in Section 5.

2 SPR joint test

Based on the part material of the steel-aluminum connection part of a certain car body, the SPR joint is carried out on the top panels made of DC01 steel (DC01) or HC280 steel (HC280) materials, and the upper beam made of 5754-H24 aluminum alloy (5754).

2.1 Material performance test of riveted sheet

2.1.1 Material constitutive model

The Johnson–Cook (J-C) model has a simple form and is often used in engineering [23]. The constitutive relation of the J–C model is shown in Eq. (1).

$$\sigma_y = (A + B\varepsilon^n) \cdot \left(1 + C \ln \frac{\dot{\varepsilon}_{eff}}{\dot{\varepsilon}_0}\right) \quad (1)$$

where σ_y is the flow stress, and its unit is MPa; $\dot{\varepsilon}_{eff}$ is the strain rate; $\dot{\varepsilon}_0$ is the quasi-static strain rate; A , B , C , and n are the constitutive fitting parameters.

During the forming process of the SPR joint, the rivet will pierce the upper sheet. Moreover, both the upper and lower

sheets may fail and fracture under tension conditions. The stress state of the sheet is different under different tensile conditions. Stress triaxiality σ^* characterizes various complex stress states of metal materials under loads in different directions [20].

The J-C failure model [24] is shown in Eq. (2).

$$\epsilon_f^{pl} = D_1 + D_2 \exp(D_3 \sigma^*) \tag{2}$$

where $D_1 \sim D_3$ are failure parameters.

2.1.2 Tensile test of riveted sheet material

The stress triaxiality of the element at the notch is calculated during the deformation process of the notched specimen [25]. According to the test method of GB/T 228.1–2010, the samples with notch radius r of 2 mm, 5 mm, 8 mm, 10 mm, and ∞ are designed. The electronic universal tensile testing machine (rated load 100 kN) is used together with the DIC VIC-2D high-speed full-field strain measurement system. First, speckle processing is performed on the specimen, and then the specimen with speckles is placed at the fixture of the tensile testing machine. The tensile speed of the machine is 5 mm/min. The high-speed camera is turned on simultaneously to collect pictures of the changes in the sample during the stretching process. The tensile testing machine collects the force–time curve, and the full-field strain system collects the displacement and strain versus time. Finally, combining the two can obtain the stress–strain curve and the full-field strain at the speckle position, as shown in Fig. 1. Each group is subjected to three tensile tests, and the data are averaged

1) Material constitutive relationship

The material tensile test of the sample with notch radius ∞ is extracted. The true stress–strain curves of DC01, HC280, and 5754 materials are obtained, as shown in Fig. 2. The basic properties of these three materials are shown in Table 1.

The J–C model is fitted to the acquired stress–strain curves using the least squares method, as shown in Eq. (3).

$$\sigma_{DC01} = 170 + 423.29 \epsilon^{0.452} \tag{3}$$

In the same way, the J-C models of HC280 and 5754 materials are obtained.

$$\sigma_{HC280} = 280 + 762.19 \epsilon^{0.476} \tag{4}$$

$$\sigma_{5754} = 170 + 175.3 \epsilon^{0.462} \tag{5}$$

2) Material fracture constitutive model

The stretching process of the notched samples is analyzed through the full-field strain system, and the full-field strain of each sample is obtained, as shown in the strain cloud diagram of Fig. 1. The strain values at the fracture locations of samples of different materials are extracted, as shown in Table 2.

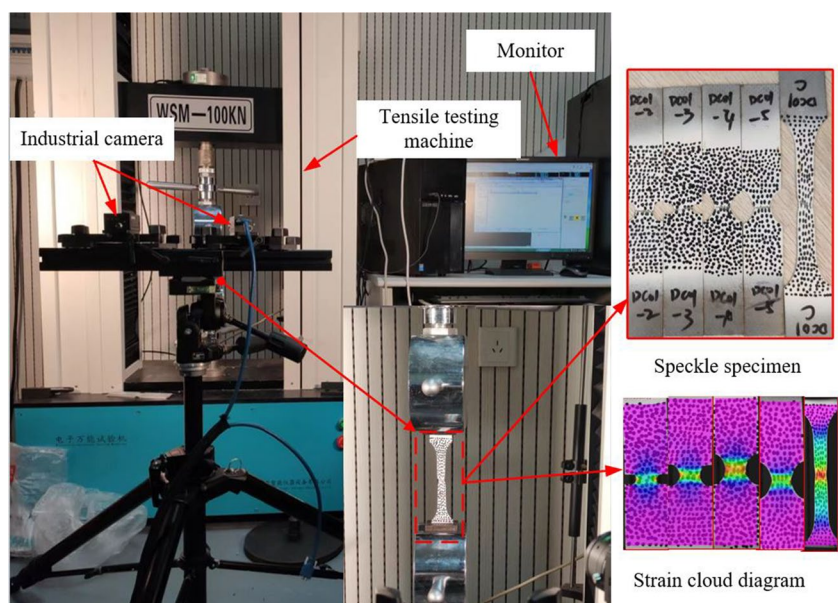
Combined with the data in Table 2, the J-C failure model is obtained by using the least square method, as shown in Fig. 3.

2.2 Forming process and performance test of SPR joint

2.2.1 SPR technology and evaluation method

When performing SPR, it is necessary to determine the type of rivet and mold according to the thickness of the

Fig. 1 Notch test of riveted sheet material



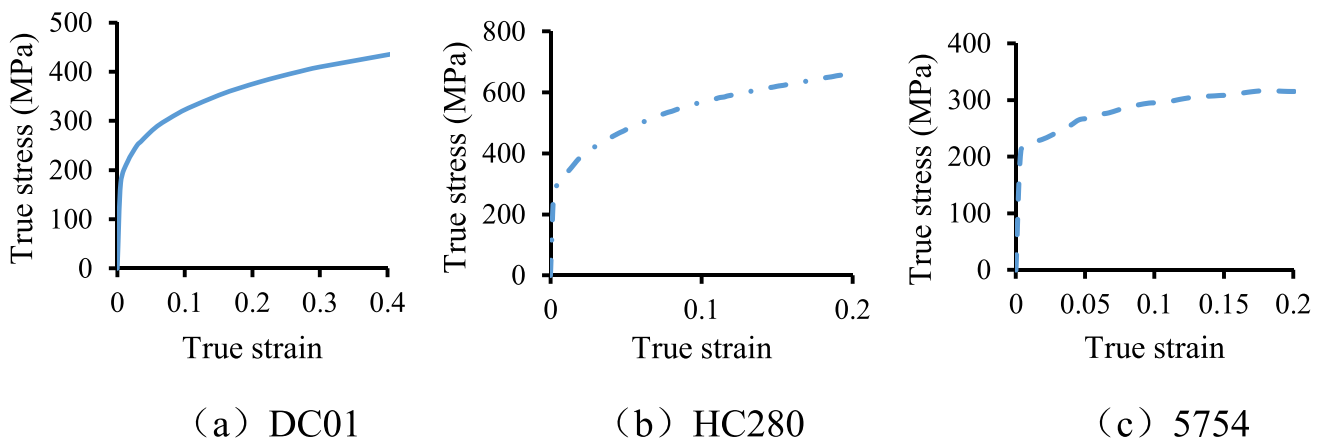


Fig. 2 True stress–strain relationship of materials

Table 1 Basic properties of materials

Material	Density	Elastic modulus	Poisson's ratio	Yield strength	Tensile strength
DC01	7850 kg/m ³	207 GPa	0.3	170 MPa	310 MPa
HC280	7850 kg/m ³	207 GPa	0.3	280 MPa	520 MPa
5754	2700 kg/m ³	70 GPa	0.33	170 MPa	250 MPa

Table 2 Stress triaxiality and failure displacement

	Specimen	Stretch	1	2	3	4
Property	<i>r</i> /mm	∞	10	8	5	2
	σ*	0.33	0.43	0.48	0.52	0.6
DC01	Fracture strain	0.574	0.45	0.39	0.357	0.306
HC280	Fracture strain	0.507	0.40	0.337	0.289	0.247
5754	Fracture strain	0.258	0.197	0.163	0.136	0.106

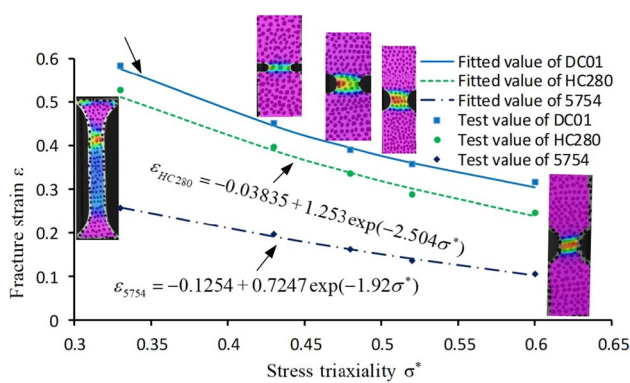


Fig. 3 Failure strains of different stress triaxiality

sheet. Considering the SPR of 1 mm DC01 and 1.7 mm 5754, a rivet with a diameter of 5.3 mm and length of 5 mm is selected, as shown in Fig. 4a. The die parameters are shown in Fig. 4b.

The evaluation methods for the connection performance of SPR joints mainly include the section evaluation method and load evaluation method. The section evaluation method judges the quality of the joint by measuring the geometric dimensions of the main shape features, as shown in Fig. 5. Among them, *u* is the interlock length, *t_b* is the bottom thickness, and *t_r* is the remaining bottom thickness. The minimum value of the bottom thickness *t_m* is the minimum value of the bottom thickness *t_b* and the remaining thickness *t_r*. The interlock length *u* and the minimum bottom thickness *t_m* are mainly selected as evaluation indicators [26]. The load evaluation method is to judge the connection performance of the joint by the tensile test.

2.2.2 SPR sample

Tensile testing of the load evaluation method includes shearing, cross-drawing, and peeling conditions. The geometric dimensions of 1mm DC01 and 1.7 mm 5754 are designed, as shown in Fig. 6a, b, and c, respectively. The

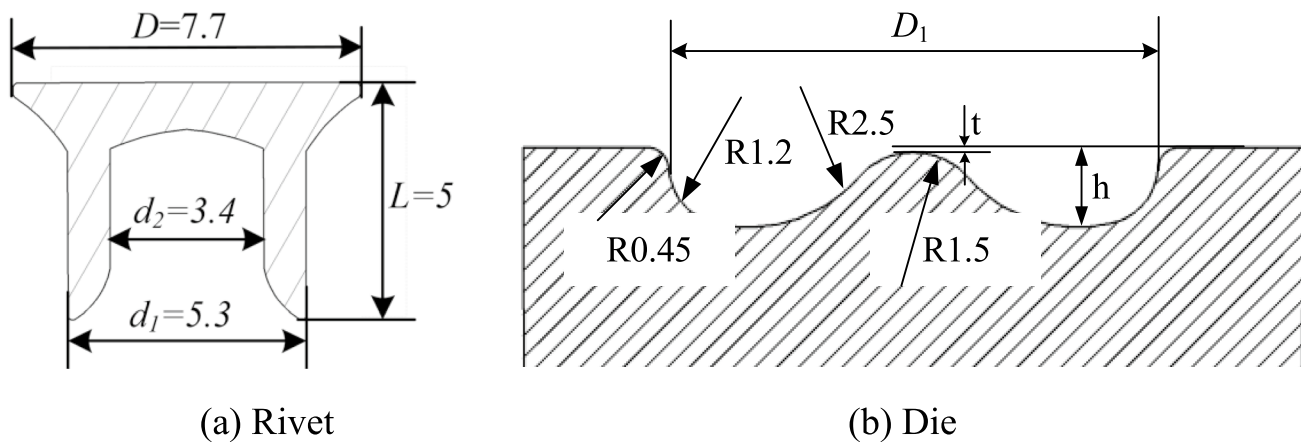


Fig. 4 Process parameters (dimensions in millimeters)

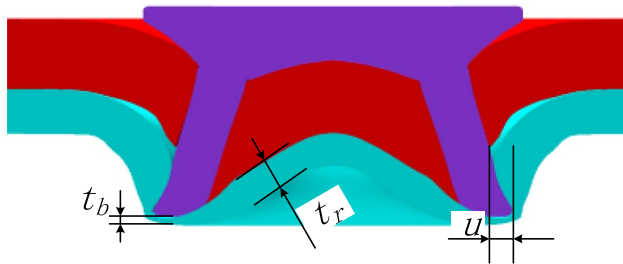


Fig. 5 Feature size of cross-sectional evaluation method

upper sheet is made of 1mm DC01 material, and the lower sheet is made of 1.7 mm 5754 material. The hole is where the clamp is secured.

2.2.3 Forming test of SPR joint

The SPR joint samples are riveted in an automatic riveting machine, in which the equipment model is EP-CTF, and the maximum riveting force is 75 kN. The upper and lower riveting sheets are first placed above the concave die of the SPR machine. The riveting machine then riveted the center of the rivet sheet positioning at a speed of 20 mm/s. The SPR samples of cross-drawing, shear, and peel joints are obtained, as shown in Fig. 7. The riveting force indicator can display the riveting pressure value.

2.3 Mechanical performance test of joint

The cross-drawing, shearing, and peeling tests are carried out on the WSM3100 microcomputer-controlled electronic universal testing machine. The tensile speed is set to 5 mm/min, as shown in Fig. 8a, b, and c.

3 Finite element analysis of SPR joint

3.1 Finite element modeling of SPR

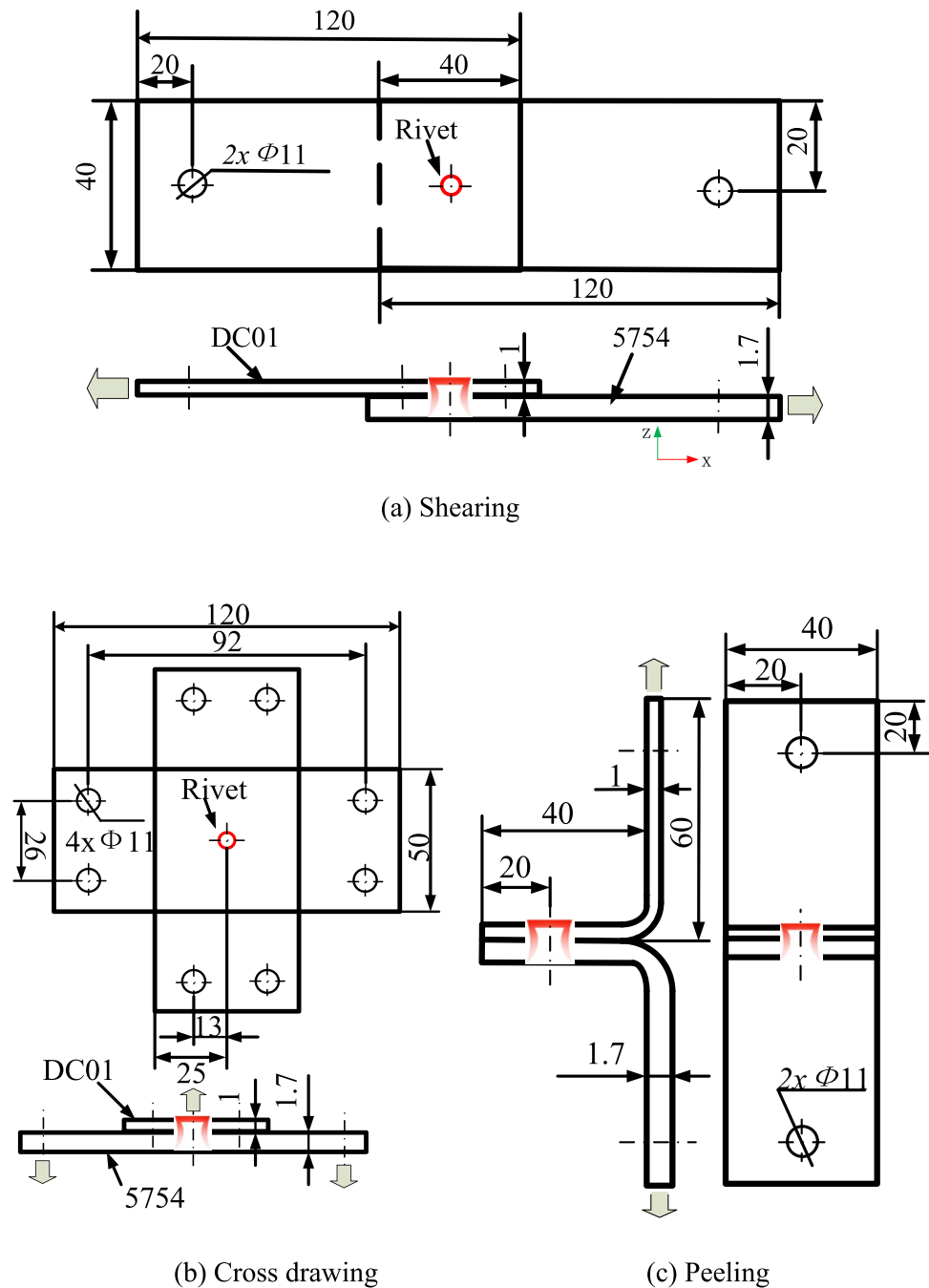
SPR forming process of 1mm DC01 and 1.7 mm 5754 material is simulated. To improve the simulation speed of riveted joint forming, a 2D axisymmetric FEM is built using commercial Simufact forming software. The steps of the SPR modeling are as follows:

First, the geometric modeling of the SPR is carried out, including punch, blank holder, rivet, upper and lower riveting sheets, and die. The upper and lower sheets are divided to generate the riveted area and the stretched area, as shown in Fig. 9a.

Then, the material constitutive model and failure model of DC01 and 5754 are assigned to the finite element model. Henrob H4 series rivets are used, and material properties are selected from the material library of software. The tension areas of the upper and lower riveted sheets are set for bonding and binding contact, and the other parts are set for automatic contact. The friction between the parts is simulated using a mixed friction model, including Coulomb friction and shear friction models. The friction coefficients of the Coulomb friction and shear friction models are set to 0.1 and 0.2, respectively. The punch, blank holder, die, and upper and lower sheet stretching areas are defined as rigid body. The pressure of the blank holder is set to 3500N.

Finally, the mesh size of 0.14mm is used for the upper and lower sheet riveting area, and a grid size of 0.05mm is used for the rivets with a secondary roughening algorithm. The element type is quadrilateral. The punch riveting speed is set to 20mm/s. The vertical distance from the punch to the upper sheet is set as the stroke of the punch, and the distance is 6.22 mm to ensure the flatness of the upper surface after riveting.

Fig. 6 Geometric dimensions of samples (dimensions in millimeters)



(a) Shearing

(b) Cross drawing

(c) Peeling

The FEM of SPR joint forming is established, as shown in Fig. 9b.

3.2 Forming quality analysis of SPR

The simulated and tested SPR joint forming evaluation indicators are measured, as shown in Fig. 10. The relative errors of the interlock length and remaining thickness are 8.21% and 2.5%, respectively, as shown in Table 3. It is good consistency between the simulation model and test in terms of SPR joint forming performance.

3.3 Mechanical performance simulation of SPR joint

3.3.1 Forming analysis of SPR joint

After the 2D model of SPR is formed, the simulation result model is rotated to generate a 3D solid model. The result data of the joint are rotated and mapped, and residual information is retained, such as residual stress and residual strain, as shown in Fig. 11. Then, the tensile mechanical performance of the joints is analyzed

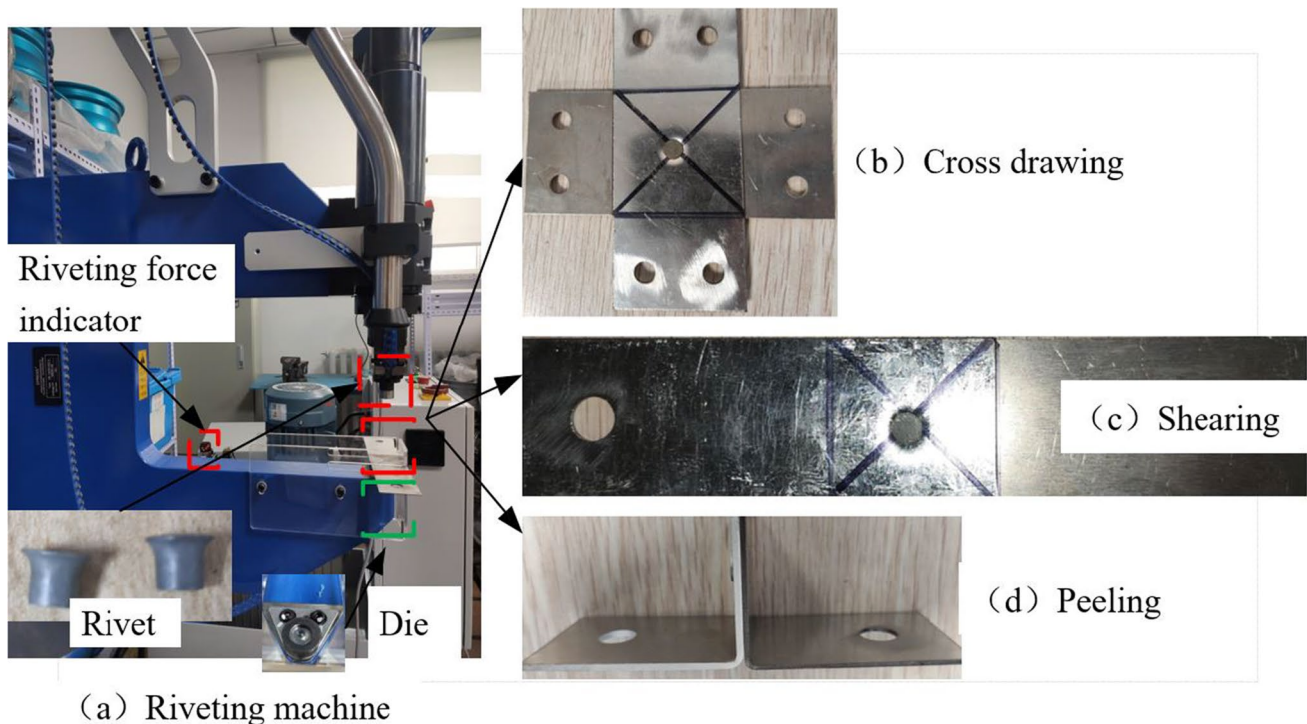


Fig. 7 SPR forming test

to realize the integrated design of the joint forming and mechanical performance simulation considering the residual information.

Referring to the cross-drawing, shearing, and peeling tensile test, the lower sheets are fixed during the simulation of the tensile mechanical performance of the SPR joint. A constant speed of 5 mm/min is applied to the upper sheet, where the load direction for the cross-drawing and peeling conditions is in the positive Z-axis direction and the shearing condition is in the positive X-axis direction. Due to the possibility of sheet tearing during the stretching process of SPR joints, the J-C material failure model is selected to simulate the sheet tearing combined with Sect. 2.1.2.

3.3.2 Failure mode analysis of joint

Compared with the test results, the simulation results of the SPR joint under three tensile conditions are extracted, as shown in Fig. 12a, b, and c.

Figure 12 shows that the failure mode of the SPR joint under the cross-drawing condition is the failure of the upper sheet to come out. This is mainly because the thickness of the upper sheet is thinner and its strength is weaker than the lower sheet. Under the action of axial tensile load along the joint, the upper sheet is concave along the joint,

and the bending angle continues to increase. The material of the upper sheet undergoes large plastic deformation at the joint position, and then the upper sheet comes out of the rivets, causing the joint to fail. This is consistent with the cross-draw test results in Fig. 12a.

The failure mode of the SPR joint under the shear condition is the failure of the lower sheet coming out. The main reason is that the load in the shear condition is loaded along the radial direction of the joint, and the rivets continue to tilt, which destroys the interlocking structure of the rivets. Finally, the upper sheet and the rivets come out together. The lower sheet is tearing due to the large interlock value. This is consistent with the shear test results in Fig. 12b.

The form of the SPR joint under the peeling condition is similar to that of the cross-drawing condition, and the upper sheet is pulled out, which leads to the failure of the joint. Since the peeling condition is axial unilateral loading, the riveted area of the lower sheet is bent simultaneously with the upper sheet and the rivet, resulting in larger deformation of the joint area on the tensile side of the upper sheet. Finally, the riveted area of the upper sheet is larger resulting in joint failure. This is consistent with the peel test results in Fig. 12c.

The force–displacement curves of the simulation and test under different tensile conditions are extracted, as shown in

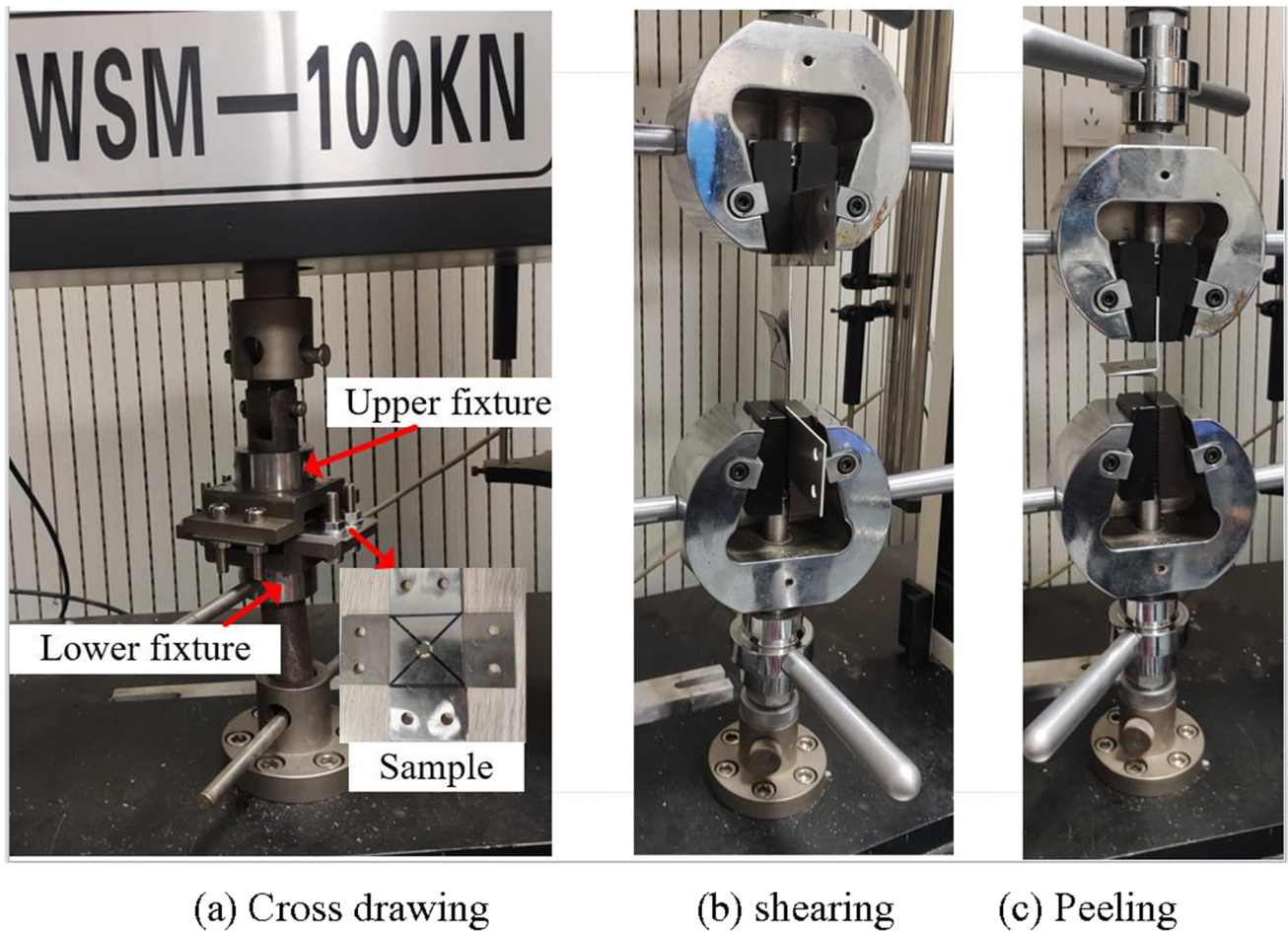


Fig. 8 Tensile test of SPR joints

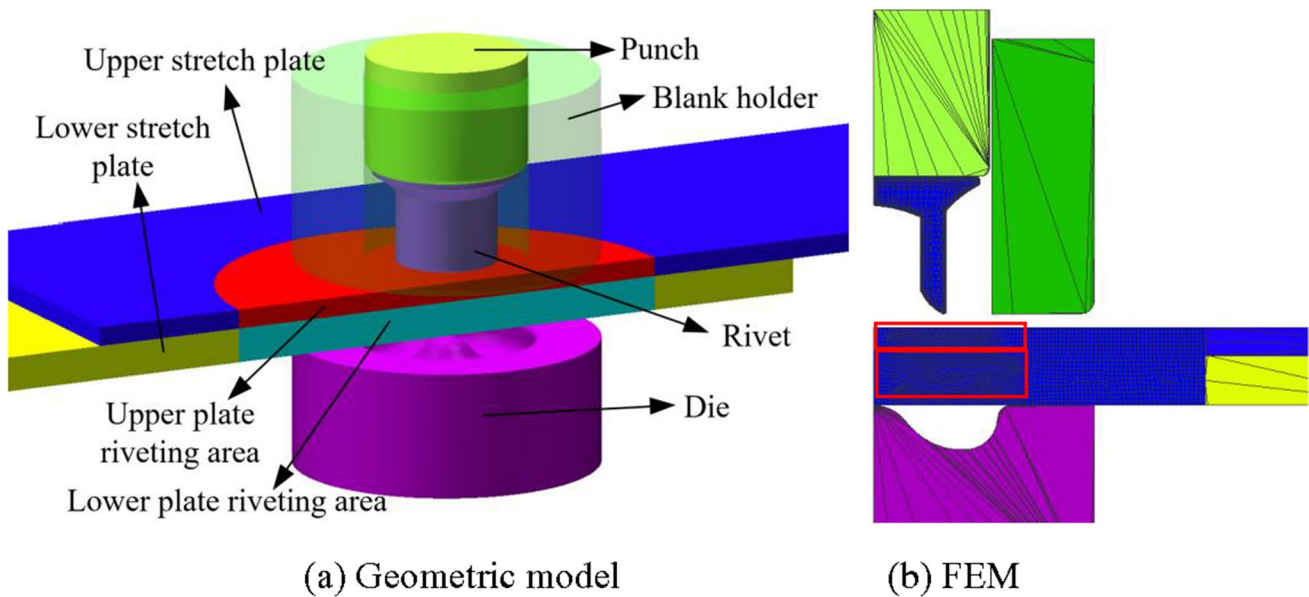


Fig. 9 Simulation model of SPR

Fig. 10 Forming evaluation index of SPR joint (dimensions in millimeters)

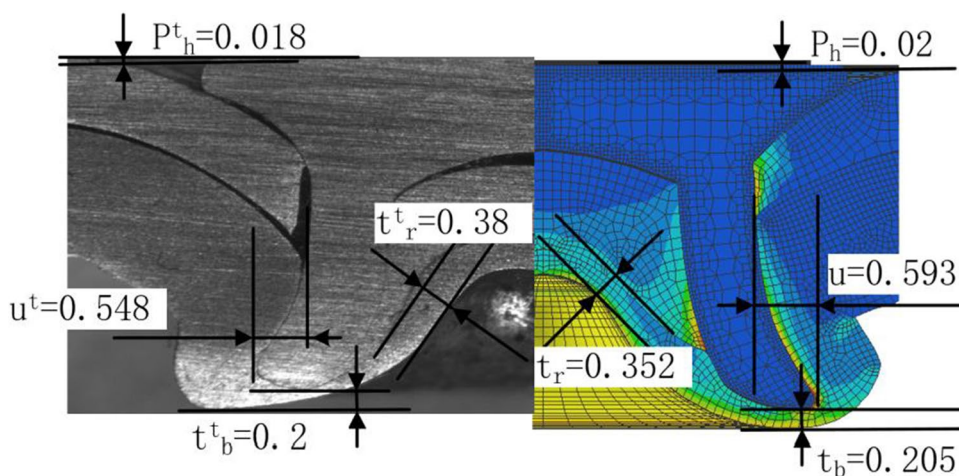


Table 3 SPR forming evaluation index

Index	Test	Simulation	Error
t_r	0.38	0.352	7.37%
u	0.548	0.593	8.21%
t_b	0.2	0.205	2.50%

Fig. 13. The simulation results are also calculated for different tensile conditions without considering the residual information.

Figure 13 shows that the tensile failure displacement considering the residual stress is larger than that without considering the residual information, and the relative error of the maximum load force is smaller. The variation trend of the simulation curve considering the residual information is consistent with the test. The relative error between the test results of the maximum cross-drawing force, shearing force, and peeling force under different tensile conditions and the simulation considering the residual information is within

10%, and the maximum relative error between the simulation and test of failure displacement is within 10%, as shown in Table 4. In the shear condition, the relative error of the failure displacement without considering the residual information is larger. Therefore, the accuracy of the SPR joint forming-cross drawing/shearing/peeling integrated analysis model considering residual information is higher than the model without considering residual information.

4 Hybrid sequence approximate optimization method of SPR process parameters

When SPR is performed on sheets of different materials and thicknesses, different rivets and molds will affect the quality and reliability of riveted joints. Therefore, it is necessary to optimize the design of the joint process to obtain the optimal rivet and die process parameters.

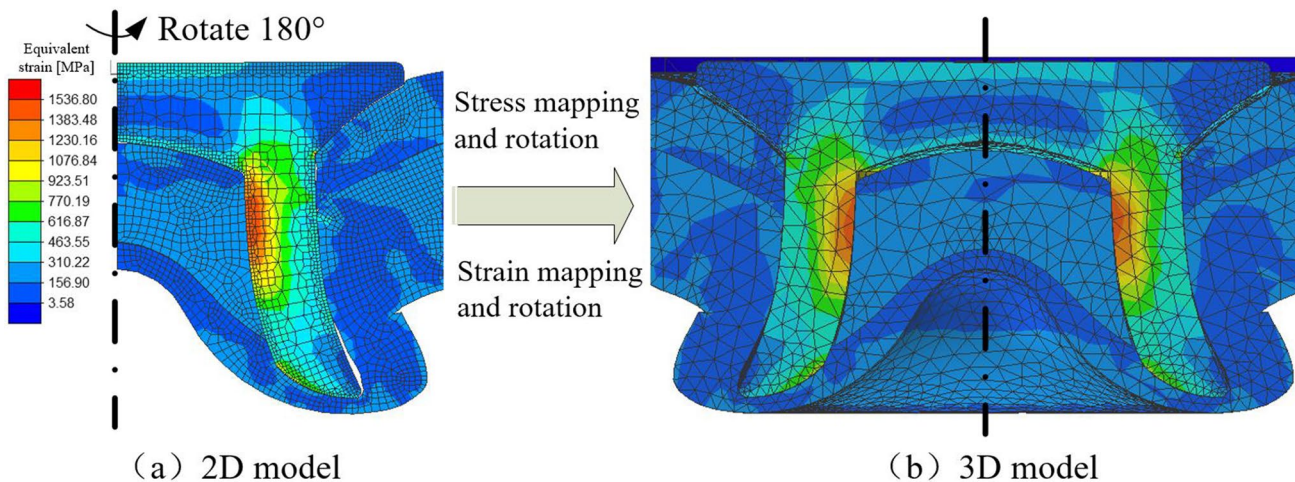


Fig. 11 Forming information mapping of SPR joint

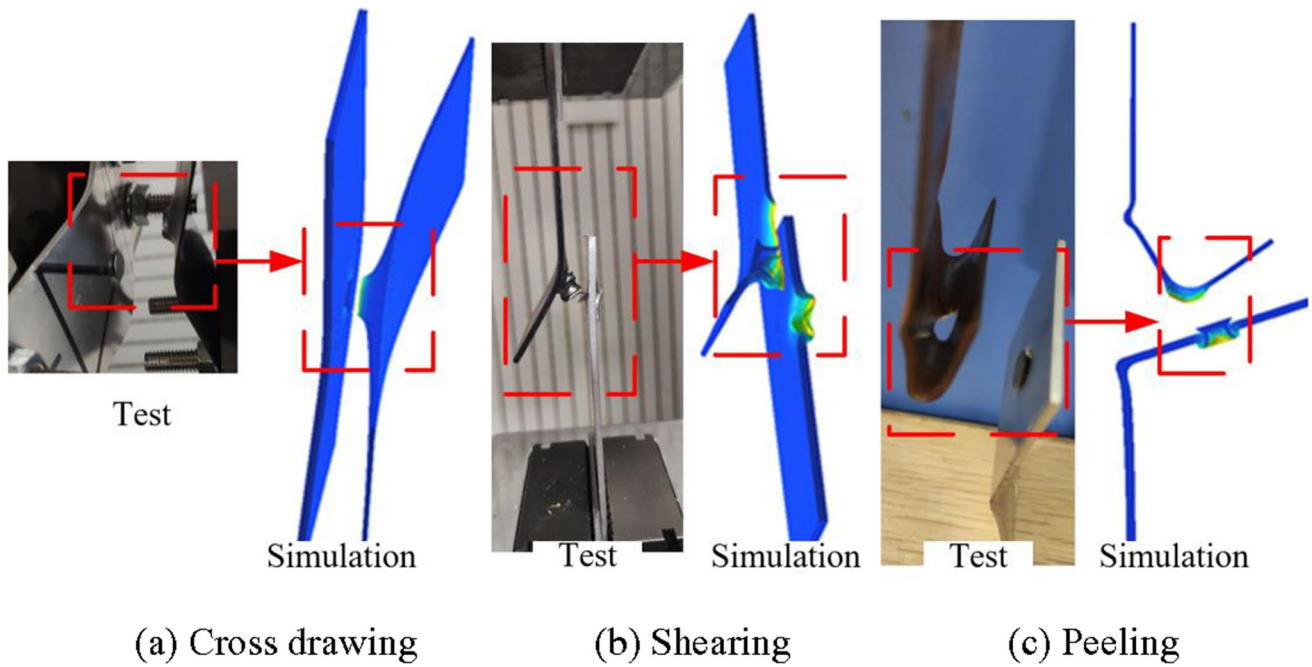


Fig. 12 Failure mode of SPR joint

Fig. 13 Mechanical performance simulation and test of joint

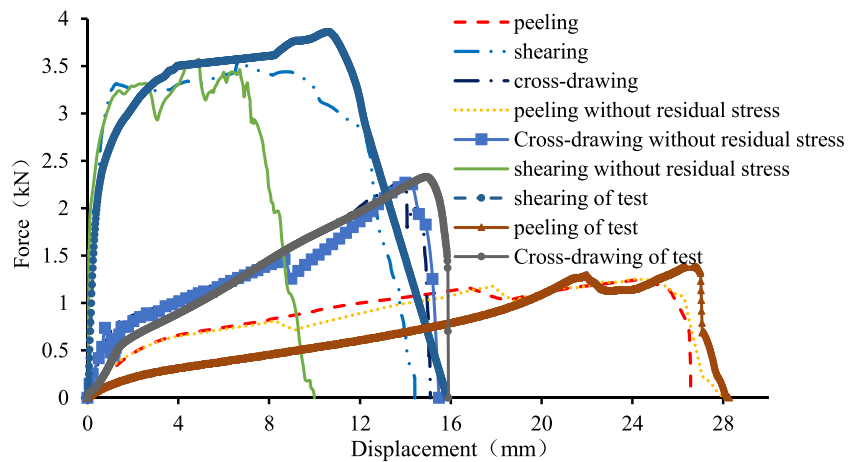


Table 4 Comparison between simulation and test

Condition	Peak force			Failure displacement		
	Test/kN	Simulation/kN	Relative error/%	Test/mm	Simulation/mm	Relative error/%
Cross-drawing	2.328	2.254	3.179	15.9	15.1	5.031
Shearing	3.86	3.556	7.876	15.86	14.42	9.079
Peeling	1.383	1.248	9.761	28.26	26.57	5.980

4.1 Hybrid sequence approximate optimization method

The simulation of forming and mechanical performance of SPR joints involves material nonlinearity, contact

nonlinearity, and solution nonlinearity, which are highly nonlinear and require a large amount of calculation. The optimization method based on the approximate model needs to pre-estimate a large number of sample points to improve the calculation accuracy. If the accuracy is not enough,

re-sampling is required, which will increase the amount of calculation, and the method cannot guarantee the accuracy of predicting the optimal solution.

Aiming at the insufficiency of the optimization method based on the approximate model, the sequential approximate optimization method can improve the optimization efficiency of the approximate model and enhance global convergence. The specific steps of the sequence approximate optimization method are as follows [22]:

Step 1: According to the design variables and design space, the optimal latin hypercube sampling method is used to sample the initial points. The number of initial sample points should not be less than the minimum sample points required to construct an approximate model, as shown in Eq. (6).

$$N \geq 2n_s + 1 \tag{6}$$

where N is the number of sample points; n_s is the dimension of design space.

Step 2: The response values of each sample point are calculated by design of experiment (DOE). The initial number of iterations is set to $k = 1$. When $k \geq 2$, the optimal solution and its response value in Step7 are extracted. Then the sample point and response library are updated;

Step 3: The sample points and their response values are extracted. The constraint responses are constructed as RSM, and the objective function response is constructed as radial basis function neural network model (RBFNN);
 Step 4: The multi-island genetic algorithm is used to globally find the optimal solution of the constructed approximate model and obtain the predicted optimal solution x_k^* of the k th iteration and the corresponding predicted response values $\tilde{f}(x_k^*)$ and $\tilde{g}(x_k^*)$;

Step 5: The optimal solution x_k^* of the k th iteration is substituted into the analytical model to obtain the objective function value $f(x_k^*)$ and the constraint value $g(x_k^*)$ of the analytical model of the k th iteration. The results are saved into the optimal solution set.

Step 6: When $k = 1$, go to Step 7 directly. When $k > 2$, by calculating the relative error of the analytical model response value of the k th iteration and the $(k-1)$ th iteration in the optimization process. By judging whether the relative error satisfies the given convergence criterion ϵ and the analysis model constraint value meets the constraint requirements, as shown in Eq. (7). If it is satisfied, stop the cycle, and the optimal solution obtained in Step 5 is the optimal solution of the analysis model. If not satisfied, go to Step 7.

$$\begin{aligned} & \left| \frac{f(x_k^*) - f(x_{k-1}^*)}{f(x_{k-1}^*)} \right| \leq \epsilon \\ & g(x_k^*) \leq g_0 \text{ or } g(x_k^*) \geq g_0 \end{aligned} \tag{7}$$

where ϵ is the convergence precision value; g_0 is the constraint reference value.

Step 7: The approximate optimal solution $f(x_k^*)$ and the value of the design variable x_k^* are used as a new set of sample points. Then return to Step 2, the new sample points are constructed, and $k = k + 1$ is set.

4.2 Design of experiment for joint parameters

The material-structure-process parameters of SPR joints are coupled together to explore the mechanical performance of the joints.

The 5754 is connected with DC01 and HC280 respectively in a car body, and the joints of the two materials are connected for DOE. The material parameters x_1 (DC01 or HC280 material) of the rivet sheet, process parameters including rivet leg length x_2 , rivet diameter x_3 , die diameter x_4 , die bottom height x_5 , and die boss height x_6 , and structural parameters including end distance x_7 and the side distance x_8 of the rivet sheet are selected as variables, as shown in Fig. 14. The levels of the variables are shown in Table 5. Other setting parameters for analytical solutions are the same as in Sect. 3.1. The performance response of SPR joints is mainly divided into riveting forming indicators (interlock length u , minimum bottom thickness t_m , and maximum riveting force F_r) and connection tensile mechanical performance indicators (maximum shear force F_s , maximum draw force F_d and the maximum peel force F_p).

When $x_1 = 1$, the steel sheet is 1mm DC01 material, the horizontal numbers 1, 2, and 3 of x_2 represent the rivet lengths of 5 mm, 5.2 mm, and 5.3 mm, respectively, and the horizontal numbers 1, 2, 3, and 4 of x_4 represent the die diameters are 4.6 mm, 4.8 mm, 5 mm, 5.2 mm; when $x_1 = 2$, the steel sheet is 2.5mm HC280 material, and the horizontal numbers 1, 2, 3 of x_2 represent the rivet lengths of 6.8 mm, 7 mm, 7.2 mm respectively, and the horizontal numbers 1, 2, 3, and 4 of x_4 represent the die diameters of 4.8 mm, 5 mm, 5.2 mm, and 5.4 mm, respectively.

The DOE of the optimal Latin hypercube method is adopted, and the joint interlock length, remaining thickness, maximum riveting force, maximum cross draw force, maximum shear force, and maximum peel force are selected as responses. The joint forming and mechanical performance integrated simulation analysis of 50 sets of schemes are carried out, and the response values of each sampling point are obtained, as shown in Table 6.

4.3 Integrated optimization method of material-structure-process-performance

To quickly find the optimal SPR process parameters and solve the problem of low calculation efficiency caused by

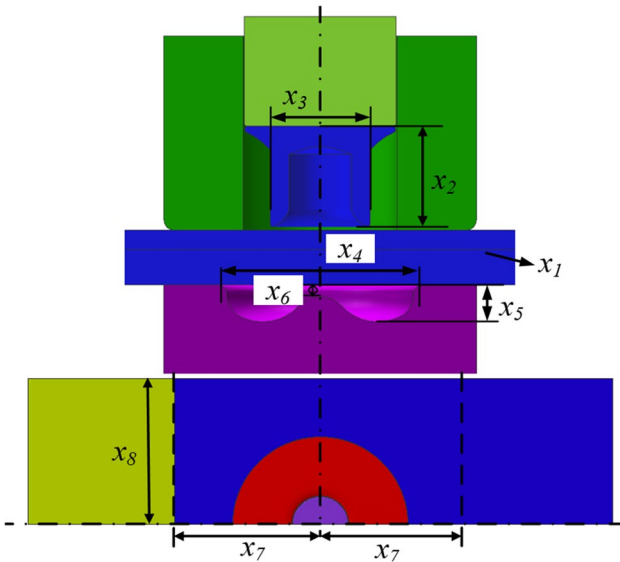


Fig. 14 Variable parameters

the multi-peak and high discreteness of the objectives and constraint functions of the connection process parameters, the structure-process-performance integrated optimization of SPR is carried out using the hybrid sequence approximate optimization method.

Since the shear strength failure is more likely to occur at the body joint, the shear strength F_s is taken as the optimization objective, and the forming quality and mechanical performance of other joints are constrained. The initial values and ranges of the design variables are according to Table 5. The mathematical model for the integrated optimization of material-structure-process-performance of SPR is as follows:

$$\begin{aligned} & \text{Find } \mathbf{x} = (x_1, x_2, x_3, \dots, x_8)^T \\ & \quad \max F_s(\mathbf{x}) \\ \text{s.t. } & \begin{cases} F_d(\mathbf{x}) \geq F_{d0}; & F_p(\mathbf{x}) \geq F_{p0}; & F_r(\mathbf{x}) \leq F_{r0} \\ u(\mathbf{x}) \geq t_{r0}; & t_m(\mathbf{x}) \geq t_{m0} \\ x_1 = 0 \text{ or } 1; & x_L \leq x_i \leq x_U \end{cases} \end{aligned} \quad (8)$$

where t_{r0} and t_{m0} are the interlock length and the minimum bottom thickness of joint forming. Considering that if the minimum thickness of the bottom is too small, it is easy to cause the lower sheet to crack or fall off, the minimum thickness is set to not less than 0.15. Since the larger the interlock length, the higher the degree of interlocking between the rivet and the lower sheet, the interlock length is set to not less than 0.2; F_{r0} , F_{d0} , and F_{p0} are the maximum riveting force, maximum pulling force, and maximum peeling force of the joint, refer to its performance before optimization, when $x_1 = 1$, F_{r0} , F_{d0} ,

Table 5 Parameter levels

Factor	Name	Description	Level			
			1 (DC01)	2 (HC280)		
Material parameter	x_1	Steel	1 (DC01)	2 (HC280)		
Process parameter	x_2	Leg length of rivet	1	2	3	
	x_3	Diameter of rivet/mm	5.1	5.3	5.5	
	x_4	Diameter of die	1	2	3	4
	x_5	Bottom height of die/mm	1.6	1.7	1.8	1.9
	x_6	Boss height of die/mm	0	0.2	0.4	0.6
	Structural parameter	x_7	Sheet end distance/mm	14	17	20
x_8		Sheet margin/mm	14	17	20	

Table 6 Results of DOE

No	x_1	x_2	x_3	x_4	x_5	x_6	x_7	x_8	Forming index/mm			Joint strength/kN		
									u	t_m	F_r	F_s	F_d	F_p
									1	0	3	5.3	4	1.8
2	1	2	5.5	3	1.7	0.4	23	14	1.321	0.469	79.430	6.538	3.292	1.363
3	1	3	5.5	3	1.8	0.4	23	23	1.388	0.303	73.335	7.119	3.198	1.539
⋮	⋮	⋮	⋮	⋮	⋮	⋮	⋮	⋮	⋮	⋮	⋮	⋮	⋮	⋮
19	0	2	5.1	3	1.7	0	23	23	0.746	0.164	32.5	4.386	3.012	1.821
20	0	3	5.1	2	1.6	0	23	23	0.943	0.134	47.989	4.171	2.856	1.593
⋮	⋮	⋮	⋮	⋮	⋮	⋮	⋮	⋮	⋮	⋮	⋮	⋮	⋮	⋮
48	1	1	5.5	3	1.9	0.6	14	14	1.165	0.316	59.052	5.786	3.560	1.803
49	0	3	5.3	4	1.6	0.4	14	17	0.94	0.131	40.280	4.031	2.645	1.619
50	1	1	5.3	4	1.6	0.2	14	14	1.201	0.406	72.107	5.749	3.632	1.794

and F_{p0} are set to 55 kN, 2.254 kN and 1.248 kN, respectively; when $x_1=2$, F_{r0} , F_{d0} , and F_{p0} are set to 73.78 kN, 3.515 kN and 1.675 kN, respectively; x_U and x_L are the upper and lower limits of the design variables, respectively.

According to the steps of the hybrid sequence approximate optimization method in Sect. 4.1 and DOE results in Sect. 4.2, the maximum shear force $F_s(x)$ is used to construct the RBFNN, and the interlock length u , the minimum bottom thickness t_m , the maximum riveting force F_r , the maximum cross draw force $F_d(x)$ and the maximum peel force $F_p(x)$ are used to construct the RSM. ϵ is set to 5%, and other optimization parameter settings are the same as in Sect. 4.1.

4.4 Results and discussion

The optimal SPR process parameters of 5754 and DC01 are obtained through hybrid sequence approximate optimization method after 2 iterations, and the optimal SPR process parameters of 5754 and HC280 are obtained through hybrid sequence approximate optimization method after 4 iterations. The final optimization results are shown in Table 7. The performance indicators of the joints are extracted, as shown in Tables 8 and 9.

Tables 8 and 9 show that the maximum relative error between the optimal value and the simulated value of each performance index based on the optimization method is less than 5%, which further illustrates the reliability of the

hybrid sequence approximate optimization method in terms of computational accuracy. After the process parameters of DC01 and 5754 riveting are optimized, the maximum cross-draw force, maximum shear force, and maximum peel force increased by 34.53%, 8.92%, and 22.43%, respectively, compared with the initial scheme. After the process parameters of HC280 and 5754 riveting are optimized, the maximum draw force, maximum shear force, and maximum peel force increased by 1.495%, 1.28%, and 6.866%, respectively, compared with the initial scheme. It shows that the hybrid sequence approximate optimization method can carry out the integrated optimization of material-structure-process-performance of SPR joints, and realize the comprehensive improvement of the comprehensive mechanical performance of joints while ensuring accuracy.

5 Conclusion

An integrated optimization method of material-structure-process performance is proposed to optimize the structure-process-performance design of SPR joints of steel/aluminum dissimilar materials. The conclusions are as follows:

- (1) Quasi-static tensile tests under different stress triaxiality states of 5754, DC01, and HC280 material are carried out. The J-C material constitutive model and

Table 7 Values of design variables after optimization

Design variable	x_1	x_2	x_3	x_4	x_5	x_6	x_7	x_8
DC01 and 5754 riveting	0	2	5.1	3	1.6	0.4	20	20
HC280 and 5754 riveting	1	3	5.1	3	1.7	0.6	20	20

Table 8 Performance index of DC01 and 5754 riveting

Performance	u/mm	t_m/mm	F_r/kN	F_s/kN	F_d/kN	F_p/kN
Initial design	0.593	0.205	55.033	3.556	2.254	1.248
Optimal value (prediction)	0.621	0.156	34.55	4.784	2.455	1.528
Optimal value (simulation)	0.648	0.1625	35.542	4.824	2.465	1.545
Relative error of prediction/%	-4.17	-4.0	-2.79	-0.83	-0.406	-1.1
Relative error of initial scheme/%	+4.72	-23.9	-37.22	+34.53	+8.92	+22.43

Table 9 Performance index of HC280 and 5754 riveting

Performance	u/mm	t_m/mm	F_r/kN	F_s/kN	F_d/kN	F_p/kN
Initial design	1.219	0.312	73.788	6.755	3.515	1.675
Optimal value (prediction)	1.317	0.520	71.48	6.839	3.556	1.752
Optimal value (simulation)	1.31	0.542	72.479	6.856	3.56	1.79
Relative error of prediction/%	-0.534	+4.022	+1.378	+0.248	+0.112	+2.123
Relative error of initial scheme/%	+7.465	+73.717	-1.774	+1.495	+1.28	+6.866

failure fracture model considering the stress triaxiality are established. The simulation analysis of joint forming is carried out, and the riveting force and forming quality dimensions are obtained by the simulation and test. Compared with the test results, the relative errors of the simulation results are all within 10%;

- (2) The integrated simulation analysis of the joint forming and mechanical performances of cross-drawing, shearing, and peeling considering the residual information is carried out. Compared with the test results, the relative error between the test and the simulation of the maximum tensile force under different tensile conditions is within 10%, and the maximum relative error between the failure displacement and the test is within 10%. The failure displacement error of the shear condition without considering the forming information is large, which indicates that the accuracy of the established simulation model is higher; and
- (3) The optimal design of joint material-structure-process parameters is carried out using the sequence approximate optimization method. Compared with the initial model, after the process parameters of DC01 and 5754 riveting are optimized, the maximum cross draw force, maximum shear force, and maximum peel force are increased by 34.53%, 8.92%, and 22.43%, respectively. After optimizing the process parameters of HC280 and 5754 riveting, the maximum cross-drawing force, maximum shear force, and maximum peel force increased by 1.495%, 1.28%, and 6.866% compared with the initial scheme, respectively.

Author contribution All authors contributed to the study conception and design. Chong Xie: investigation, conceptualization, writing—original draft, revision, figure arrangement. Dengfeng Wang: resources. Dewen Kong: validation. Shuang Wang: data curation. Changqing Du: resources, supervision.

Funding This work was supported by the National Key Research and Development Project of China [2022YFB2503501], the National Natural Science Foundation of China [51975244], the Key Scientific Research Project Plan in Henan Province [23A460025], and the Graduate Innovation Fund of Jilin University [101832020CX131].

Data availability Not applicable.

Declarations

Ethics approval The present manuscript has not been published elsewhere, and publication has been approved by the co-author.

Competing interests The authors declare that they have no known competing financial interests or personal relationships that could have appeared to influence the work reported in this paper.

References

1. Manladan S, Yusof F, Ramesh S, Fadzil M, Luo Z, Ao S (2017) A review on resistance spot welding of aluminum alloys. *Int J Adv Manuf Technol* 90:605–634
2. Du Z, Wei B, He Z, Cheng A, Duan L, Zhang G (2021) Experimental and numerical investigations of aluminium–steel self-piercing riveted joints under quasi-static and dynamic loadings. *Thin-Walled Struct* 169:108277
3. Li L, Jiang H, Zhang R, Luo W, Wu X (2022) Mechanical properties and failure behavior of flow-drilling screw-bonding joining of dissimilar aluminum alloys under dynamic tensile and fatigue loading. *Eng Fail Anal* 139:106479
4. Shi C, Li H, Chen C, Ouyang Y, Qin D (2022) Experimental investigation of the flat clinch–rivet process. *Thin-Walled Struct* 171:108612
5. Mucha J (2011) A study of quality parameters and behaviour of self-piercing riveted aluminium sheets with different joining conditions. *Strojniški Vestnik-J Mech Eng* 57(4):323–333
6. Franco Di, Fratini L, Pasta A, Ruisi V (2013) On the self-piercing riveting of aluminium blanks and carbon fibre composite panels. *Int J Mater Form* 6:137–144
7. Ang H (2021) An overview of self-piercing riveting process with focus on joint failures, corrosion issues and optimisation techniques. *Chin J Mech Eng* 34(1):1–25
8. Mori K, Abe Y, Kato T (2012) Mechanism of superiority of fatigue strength for aluminium alloy sheets joined by mechanical clinching and self-pierce riveting. *J Mater Process Technol* 212(9):1900–1905
9. Atzeni E, Ippolito R, Settineri L (2009) Experimental and numerical appraisal of self-piercing riveting. *CIRP Ann* 58(1):17–20
10. Abe Y, Kato T, Mori K (2009) Self-piercing riveting of high tensile strength steel and aluminium alloy sheets using conventional rivet and die. *J Mater Process Technol* 209(8):3914–3922
11. Porcaro R, Hanssen A, Langseth M, Aalberg A (2006) The behaviour of a self-piercing riveted connection under quasi-static loading conditions. *Int J Solids Struct* 43(17):5110–5131
12. Hanssen A, Olovsson L, Porcaro R, Langseth M (2010) A large-scale finite element point-connector model for self-piercing rivet connections. *Eur J Mech-A/Solids* 29(4):484–495
13. Xue Z, Wang X, Xu C, Chen Z, Feng X, Zhou Q, Li L (2023) Equivalent characterization of pre-strained material properties and mechanical behavior prediction of steel/aluminum self-piercing riveted joints. *Thin-Walled Struct* 182:110243
14. Hassanifard S, Adibeig M, Mohammadpour M, Varvani-Farahani A (2019) Fatigue life of axially loaded clamped rivet-nut joints: Experiments and analyses. *Int J Fatigue* 129:105254
15. Karathanasopoulos N, Pandya K, Mohr D (2021) An experimental and numerical investigation of the role of rivet and die design on the self-piercing riveting joint characteristics of aluminum and steel sheets. *J Manuf Process* 69:290–302
16. Jin X, Li Y, Lou M, Wang Y (2011) Process optimization of self-piercing riveting aluminum to high strength steel using DOE method. *Chin J Automot Eng* 1(3):185–191
17. Zhao H, Han L, Liu Y, Liu X (2021) Modelling and interaction analysis of the self-pierce riveting process using regression analysis and FEA. *Int J Adv Manuf Technol* 113:159–176
18. Zhang Y, Shi B, Zhong J (2020) Multi-parameter joint optimization of self-piercing riveting on aluminum alloy plate. *J Phys: Conf Ser* 1605:012093
19. Zhao H, Han L, Liu Y, Liu X (2021) Quality prediction and rivet/die selection for SPR joints with artificial neural network and genetic algorithm. *J Manuf Process* 66:574–594

20. Fang Y, Huang L, Zhan Z, Huang S, Liu X, Chen Q, Han W (2022) A framework for calibration of self-piercing riveting process simulation model. *J Manuf Process* 76:223–235
21. Wang D, Kong D, Xie C, Li S, Zong L (2022) Study on the effect of rivet die parameters on joint quality of self-piercing riveting employed 3D modeling and MCDM method. *Int J Adv Manuf Technol* 119(11–12):8227–8241
22. Wang D, Xie C (2022) An efficient hybrid sequential approximate optimization method for problems with computationally expensive objective and constraints. *Eng Comput* 38(1):727–738
23. Ducobu F, Rivière-Lorphèvre E, Filippi E (2017) On the importance of the choice of the parameters of the Johnson-Cook constitutive model and their influence on the results of a Ti6Al4V orthogonal cutting model. *Int J Mech Sci* 122:143–155
24. Khare S, Kumar K, Choudhary S, Singh P, Verma R, Mahajan P (2021) Determination of Johnson–cook material parameters for armour plate using DIC and FEM. *Met Mater Int* 27:4984–4995
25. Zeng L, Xia Y, Zhao H, Zhou Q (2013) On utilization of material failure criterion in modeling pull-out failure of spot-welded joints. *ASME Int Mech Eng Congr Exposition* 56383:V009T10A094
26. Du Z, Duan L, Jing L, Cheng A, He Z (2021) Numerical simulation and parametric study on self-piercing riveting process of aluminium–steel hybrid sheets. *Thin-Walled Struct* 164:107872

Publisher's Note Springer Nature remains neutral with regard to jurisdictional claims in published maps and institutional affiliations.

Springer Nature or its licensor (e.g. a society or other partner) holds exclusive rights to this article under a publishing agreement with the author(s) or other rightsholder(s); author self-archiving of the accepted manuscript version of this article is solely governed by the terms of such publishing agreement and applicable law.